DIGITAL LIGHT PROCESSING 3D PRINTING OF CERAMIC-RESIN COMPOSITE MATERIALS

Bianca-Andreea OLTEANU[1], Ciprian PREDA[1], Maria-Felicia DONDEA[1], Daniela MANOLE[1], Aura-Cătălina MOCANU[1], Florin MICULESCU[1*]

This paper presents an innovative methodology for manufacturing customized osteosynthesis screws via Digital Light Processing (DLP) 3D printing, utilizing acomposite material based on a photopolymerizable resin and hydroxyapatite (HA). A key novelty is the exclusive use of naturally derived bioceramics, successfully incorporating up to 20 wt.% bovine-derived HA into the polymer matrix. Evaluations via Scanning Electron Microscopy and Energy-Dispersive X-ray Spectroscopy (SEM-EDS), alongside ImageJ processing identified 3 wt.% HA as the optimal concentration that maximizes uniform ceramic dispersion without particle agglomeration. These findings demonstrate that combining high-resolution photopolymerization with natural HA provides an effective strategy for developing bioactive medical devices.

Keywords: additive manufacturing; Digital Light Processing (DLP); ceramic-polymer composites; hydroxyapatite; vat photopolymerization

1. Introduction

In recent decades, 3D printing technology has experienced an expansion, becoming a transformative force across a wide range of industrial sectors [1]. Additive manufacturing handles complex production tasks, which is why it is now widely adopted in fields ranging from aerospace and automotive to electronics and defense [2, 3]. Alongside these widespread industrial applications, in the biomedical sector, additive manufacturing paradigms allow for the creation of complex, patient-specific structures with unprecedented precision and efficiency, revolutionizing fields such as tissue engineering, regenerative medicine, and the fabrication of customized medical devices [3, 4].

Alongside these widespread industrial applications, in the biomedical sector, additive manufacturing paradigms allow for the creation of complex, patient-specific structures with unprecedented precision and efficiency [5, 6]. Specific medical applications include the fabrication of 3D printed cranial implants, customized internal bone fixators for orthopedics, as well as the development of

* Corresponding author, Prof. Florin Miculescu, e-mail: florin.miculescu@upb.ro
[1], Dept. of Metallic Materials Science, Physical Metallurgy, NUST POLITEHNICA Bucharest, Romania

complex 3D porous scaffolds used in tissue engineering and bone regeneration [7, 8].

Despite its manufacturing advantages, the widespread biomedical application of commercial photopolymerizable resins for long-term, direct in vivo contact is heavily restricted [4]. The main limitations derive from their general lack of bioactivity and the inherent brittleness or potential cytotoxicity of certain photo-cured networks [3, 4]. To fix these issues, researchers are increasingly turning to organic-inorganic composites [8, 9]. Hydroxyapatite, a bioceramic material chemically similar to the mineral phase of human bone tissue, is recognized for its excellent biocompatibility and osteoconductivity [8]. Blending HA into polymer matrices helps neutralize acidic byproducts and allows the implant to chemically bond with real bone, which speeds up osteointegration and lowers rejection risks [10, 11]. Beyond medical uses, industries also value HA as a reinforcement material because of its hardness, chemical stability, and thermal resistance greatly improve the mechanical properties of polymers [12]. Even with these benefits, manufacturing the composite remains difficult [13]. It is hard to evenly mix a hydrophilic ceramic powder into a hydrophobic liquid resin, and the particles usually clump together, creating structural weak spots in the final product [12, 13].

Among vat photopolymerization techniques, DLP stands out as a highly efficient additive manufacturing method. Unlike conventional point-by-point scanning systems, DLP relies on a digital projector to simultaneously illuminate and cure an entire cross-section of the photosensitive resin layer. This planer projection mechanism significantly reduces priting times while maintaining exceptional manufacturing accuracy. The selection of this specific technology for fabricating the osteosynthesis screws directly relates to its superior capability to produce complex, high-resolution 3D architectures [2,3].

The main objective of this research is to create customized osteosynthesis screws by DLP technology, utilizing a composite based on naturally-derived photopolymerizable resin and bovine-derived HA. This study aims to understand how the material composition influences the morphological and elemental characteristics of the final printed products.

2. Materials and Methods

2.1. Samples Preparation

The materials involved in the experimental phase for the synthesis of the composite biomaterial consisted of a commercial PLA-based photopolymerizable resin, acting as the polymer matrix, and natural HA derived from bovine bones, to serve as the ceramic reinforcing phase [2, 14, 15]. The HA powder was obtained from fresh bovine bones using a standard extraction protocol, extensively detailed in previously published studies [16]. This methodology involved preliminary

preparation of the bones through mechanical cleaning to remove macroscopic soft tissues and impurities, succeeded by a degreasing step using organic solvents. Subsequently, the degreased bones were subjected to a sequence of thermal treatments at high temperatures to completely eliminate the organic matter [17, 18]. Finally, the remaining mineral phase was milled and granulometrically sorted to obtain the fine HA powder that was further incorporated into the commercial PLA-based resin [19, 20]. To achieve a homogeneous dispersion an ultrasonic homogenization technique was employed [13, 21]. The HA powder was added to the resin in four different mass concentrations: 1 wt.%, 3 wt.%, 5 wt.%, and 20 wt.%. Fig. 1 displays the process of ultrasonication. The ultrasonication time was correlated with the HA concentration to prevent sedimentation and ensure homogeneity.

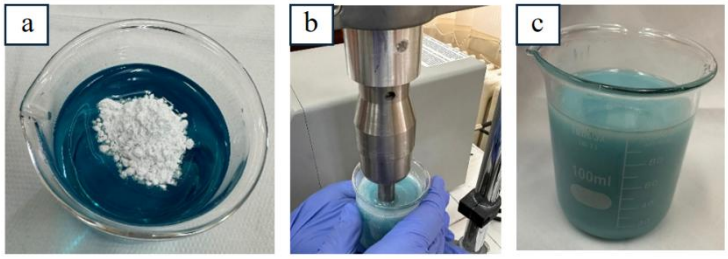

d Sample Code	HA Concentration (wt.%)	Ultrasonication Time
HA-1	1	1 min 30 s
HA-3	3	2 min 30 s
HA-5	5	4 min
HA-20	20	6 min

Fig. 1. Preparation process of the homogeneous composite resin solutions: (a) addition of HA powder to the photopolymer resin; (b) ultrasonication process for optimal particle dispersion; (c) the resulting homogeneous composite solution; (d) sample codification and specific ultrasonication times based on HA concentration.

The required amount of HA was calculated using the following formulas [11]:

$$\frac{12}{100} \times m_{solution} = m_{polymer} \quad (1)$$

$$\frac{20}{100} \times m_{polymer} = m_{HA}, \quad (2)$$

where $m_{solution}$ is the mass of the polymer solution (g), $m_{polymer}$ is the final mass of the polymer (g), and m_{HA} is the mass of the HA powder required for the 20 wt.% sample (g).

The polymers were placed in Berzelius beakers up to 100 ml, meaning 110 g (1 ml=1 cm^3; ρ=1.1 g/ cm^3). For the parts with 20 wt.% HA, the same formula was applied, but for 40 ml (see Table 1).

Table 1

The necessary amounts of HA for different volumes of composite material

HA Concentration (wt.%)	Sample Volume (ml)	Total Mass (g)	Final HA Amount (g)
1	100	110	1.1
3	100	110	3.3
5	100	110	5.5
20	40	44	8.8

2.2. CAD Modelling and DLP 3D Printing

Two distinct medical device geometries, with standard dimensions, were designed using Autodesk Inventor software: Geometry 1 represents a dental osteosynthesis screw, and Geometry 2 represents an orthopaedic screw. The digital models were exported as STL files and imported into the LycheeSlicer software to generate the necessary support structures and configure the printing parameters.

The printing parameters were set to ensure structural integrity and high resolution, as detailed in Fig. 2.

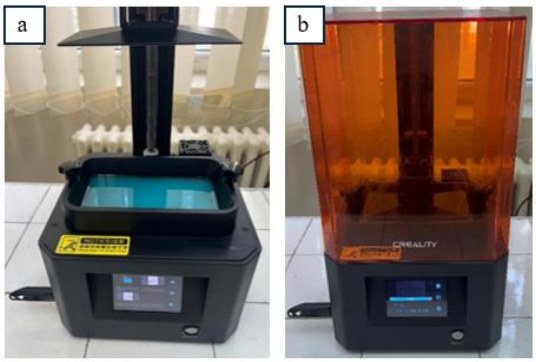

c		
	Layer thickness	50 μm
	Exposure time for the first layer	70s
	Exposure time for layers	7s
	Printing speed	23mm/s

Fig. 2. The 3D printing setup: (a) the 3D printer before the process; (b) the printer during execution; and (c) the set printing parameters

To fabricate the samples, the DLP method was used, which fundamentally relies on localized photopolymerization. By applying targeted UV light, the system cures the composite resin layer-by-layer. After concluding the printing cycle, the build platform was extracted, and the resulting composite specimens were submerged into an ethanol bath for 30 minutes. This washing step is designed to effectively dissolve and wash away any residual, uncured liquid resin. It is important to note that immediately after the primary printing program, the photopolymerizable resin is only partially solidified under the influence of the

printer's internal UV light. Consequently, the newly printed specimens exist in a relatively soft, highly deformable "green" state, lacking their ultimate structural integrity. To overcome this and achieve a complete conversion of the unreacted monomers, the specimens were subsequently placed in a dedicated UV curing chamber for 2 minutes, see Fig. 3. This supplementary UV exposure is strictly required to maximize the cross-linking density, fully solidify the composite material, and stabilize the precise mechanical dimensions of the implants, thereby preventing any subsequent structural deformations.

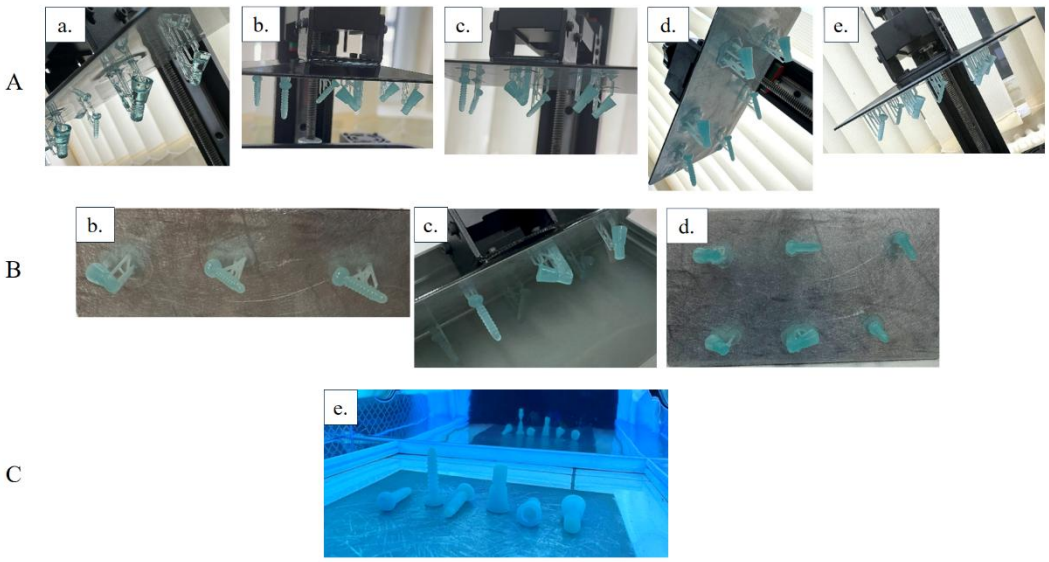

Fig. 3. Comparative overview of composite products obtained after DLP printing and the subsequent required steps: A - the samples immediately after finishing the printing process, a. the samples with 100% resin, b. samples HA-1, c. samples HA-3, d. samples HA-5, e. samples HA-20; B - samples b., c. and d. immersed in ethanol to clean them of the remaining resin; C - sample e. in the UV lamp

2.3. Samples characterization

To thoroughly evaluate the physical, microstructural, and chemical properties of the 3D printed composite materials, a comprehensive characterization protocol was conducted. The evaluation of the samples was divided into three main sequential analyses, providing both qualitative and quantitative insights into the biomaterial's structure:

(i) Morphological analysis: SEM was employed to investigate the surface topography and the morphological features of the printed composites. To get a clear view of the structure, Backscattered Electron (BSE) was used. This detector creates contrast based on atomic number (Z) differences. Because the natural HA particles contain heavier elements like calcium (Ca) and phosphorus (P), they show up much brighter in the micrographs than the lighter carbon (C) and oxygen (O) from the

PLA-based resin. This contrast allows to easily check how evenly the ceramic powder is dispersed, see exactly how the HA embeds into the polymer, and spot any micro-agglomerations [22].

(ii) Compositional analysis: EDS was utilized in conjunction with SEM to determine the precise elemental composition of the samples [23].

(iii) ImageJ quantitative analysis: For a quantitative assessment, the obtained SEM micrographs were further processed using the ImageJ open-source software, an advanced tool for scientific image analysis. For the composite samples, specific binarization (thresholding) steps isolated the HA particles from the polymer matrix and filtered out visual noise. This computational approach measured the ceramic dispersion degree and pinpointed potential agglomeration zones within the material, delivering reliable and reproducible evaluation [24].

3. Results and discussion

Scanning Electron Microscopy was used to characterize the morphology of the composites given in Fig. 4. The imaging covered two different medical geometries, contrasting lower HA additions (1 wt.% and 3 wt.%) against higher ones (5 wt.% and 20 wt.%). For the 1 wt.% and 3 wt.% mixtures, the micrographs showed a very open spread of the ceramic powder throughout the photopolymerizable resin. Despite the natural incompatibility between hydrophilic HA and hydrophobic PLA, the components bonded well, leaving the interface free of micro-agglomerations. Finding such a uniform structure confirms that the initial mechanical mixing steps worked exactly as intended before the printing process.

Increasing the HA content to 5 wt.% and then 20 wt.% changed the dispersion behavior entirely. Because the ceramic amount exceeded the polymer matrix's capacity to absorb it equally, the HA particles grouped into large micro-agglomerations. These dense clusters create weak points that concentrate stress, which can compromise the mechanical performance of the biomaterial when placed under physiological loads. In addition, the geometries directly affected the printing quality and material distribution. Across all tested mixtures, Geometry 1 allowed for a better and more uniform integration of the ceramic powder compared to Geometry 2 (Fig. 4). This behavior suggests that the specific internal architecture of Geometry 1 interacts more favorably with the rheological properties of the highly loaded resin during DLP layer-by-layer curing.

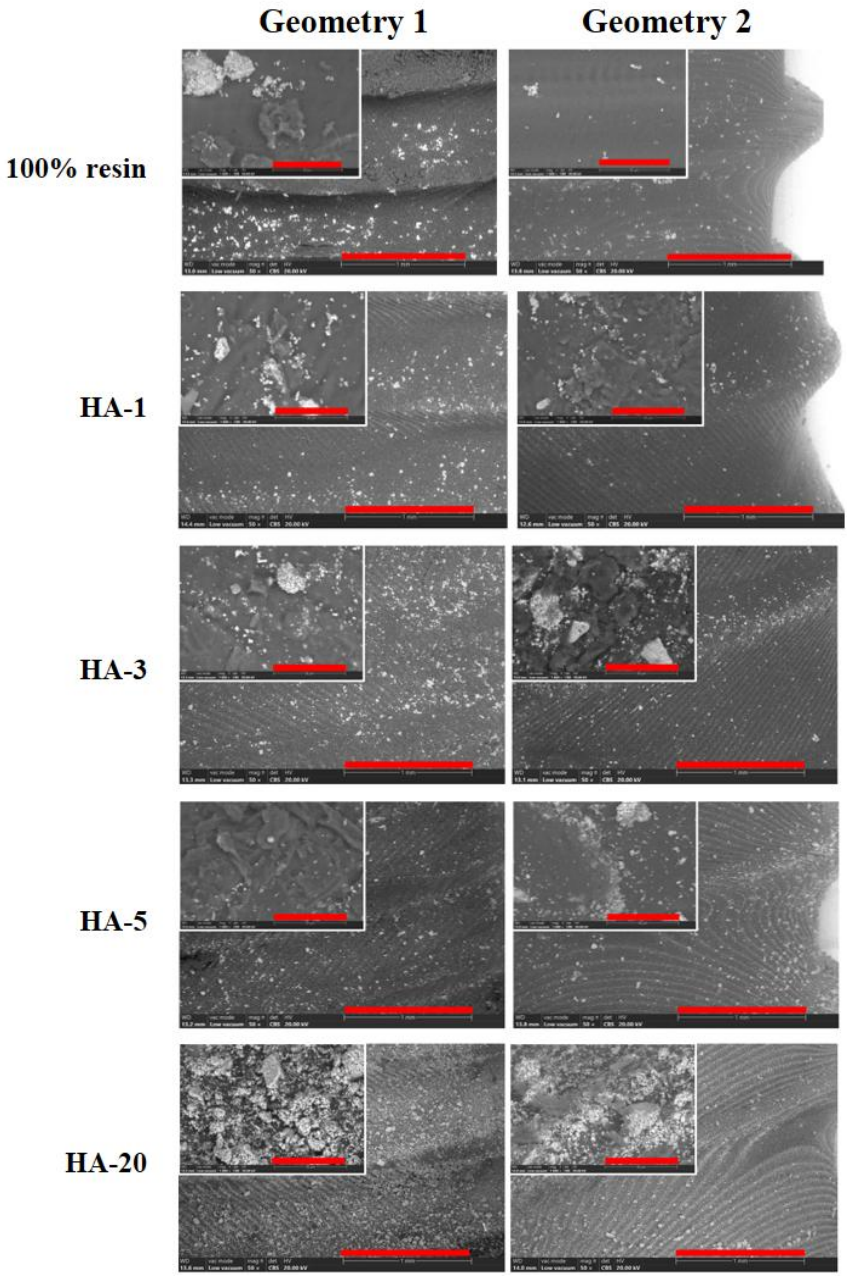

Fig. 4. Comparative representation of the morphological results for the 3D printed composite products with two geometries. Scale bar: background – 1 mm, inset – 50 μm.

Nevertheless, although both architectural designs suffered from significant localized macroscopic agglomerations at the 20 wt.% limit, the overall embedding

of the bioactive ceramic phase within the bulk structure remained extensive, successfully preserving the morphological integrity of the composites.

Alongside the major peaks for C and O corresponding to the baseline polymer, the EDS spectrum confirmed the consistent presence of Ca and P in all composite samples, validating the successful mechanical incorporation of the HA particles into the PLA matrix (see Fig. 5).

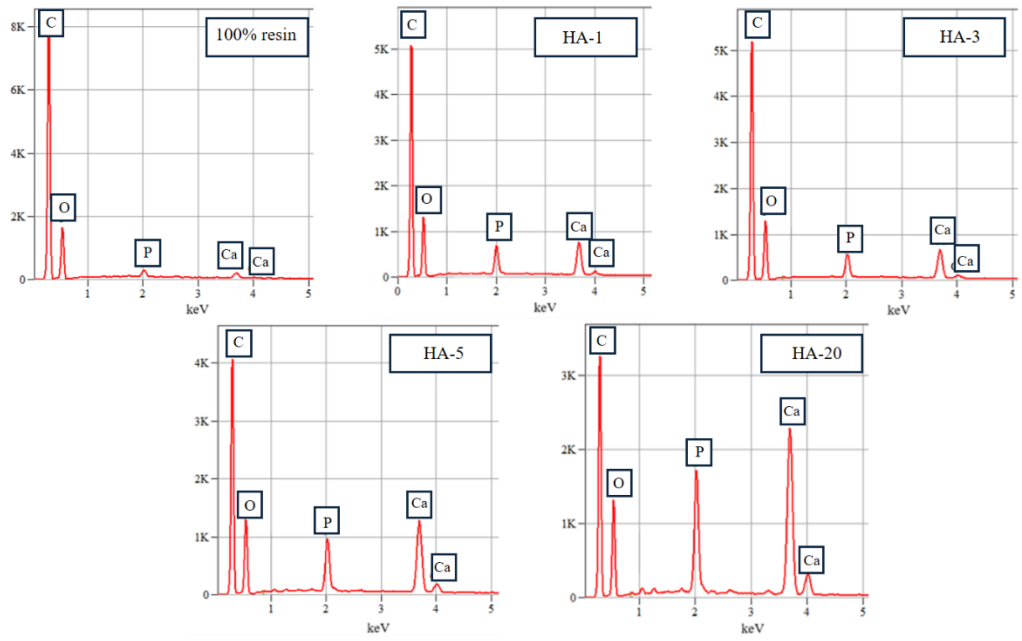

Fig. 5. Comparative representation of the EDS spectra for the 3D printed composite products

Significantly, the elemental concentrations of Ca and P extracted from the EDS profile increased proportionally to the initial HA mass percentage added to the mixtures. This proportionality demonstrates the high efficacy of the ultrasonic homogenization method employed during the pre-processing stage to ensure a uniform ceramic-polymer blend.

Graphing the elemental concentrations obtained from the EDS spectra against the HA mass fraction provides a detailed quantitative look at the composite's chemical profile (see Fig. 6). The results highlight a clear, direct proportionality. Essentially, the detected levels of Ca and P rise steadily alongside the initial amount of the added bioceramic phase.

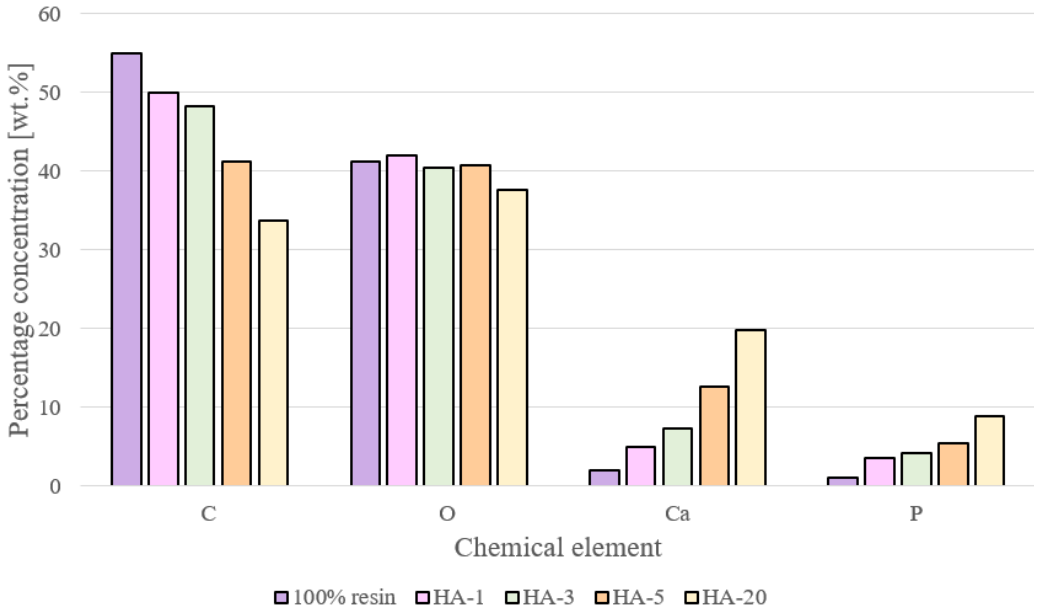

Fig. 6. The elemental concentrations corresponding to each printing set resulting from the EDS analysis

Extracting precise measurements from the SEM micrographs involved digital analysis via ImageJ (Fig. 7 and Fig. 8). By applying targeted thresholding functions, the software separated the HA particles from the background and created noise-free binary images. To further clarify the boundaries of the ceramic inclusions, the isolated HA maps were digitally colored in red. This specific segmentation routine made it possible to accurately determine the dispersion degree and the surface area fraction occupied by the ceramic material.

Quantitative evaluations of the SEM micrographs (captured at 200X magnification) on the baseline 100% resin samples showed a minimal deviation of just 1.612 μm. This value represents less than 5% of the intended 50 μm theoretical layer thickness set for the printing process. Such a small error margin proves the high dimensional accuracy and reliability of the DLP 3D printer for manufacturing high-resolution medical structures.

Defining the dispersion degree of the HA particles relies on calculating their area coverage (expressed as a percentage). As Fig. 9 illustrates, processing 200X magnification SEM images (300 μm scale bar) provides the necessary structural data. Segmenting these micrographs makes it possible to locate and precisely evaluate the distribution of the ceramic reinforcing phase inside the polymer matrix. A color mapping step then highlights the isolated HA particles in red, increasing visual contrast to sharply define the boundaries of the ceramic inclusions. Ultimately, this specific image analysis routine yields a reliable and consistent

measurement for the area fraction of the bioactive ceramic phase across all tested composites.

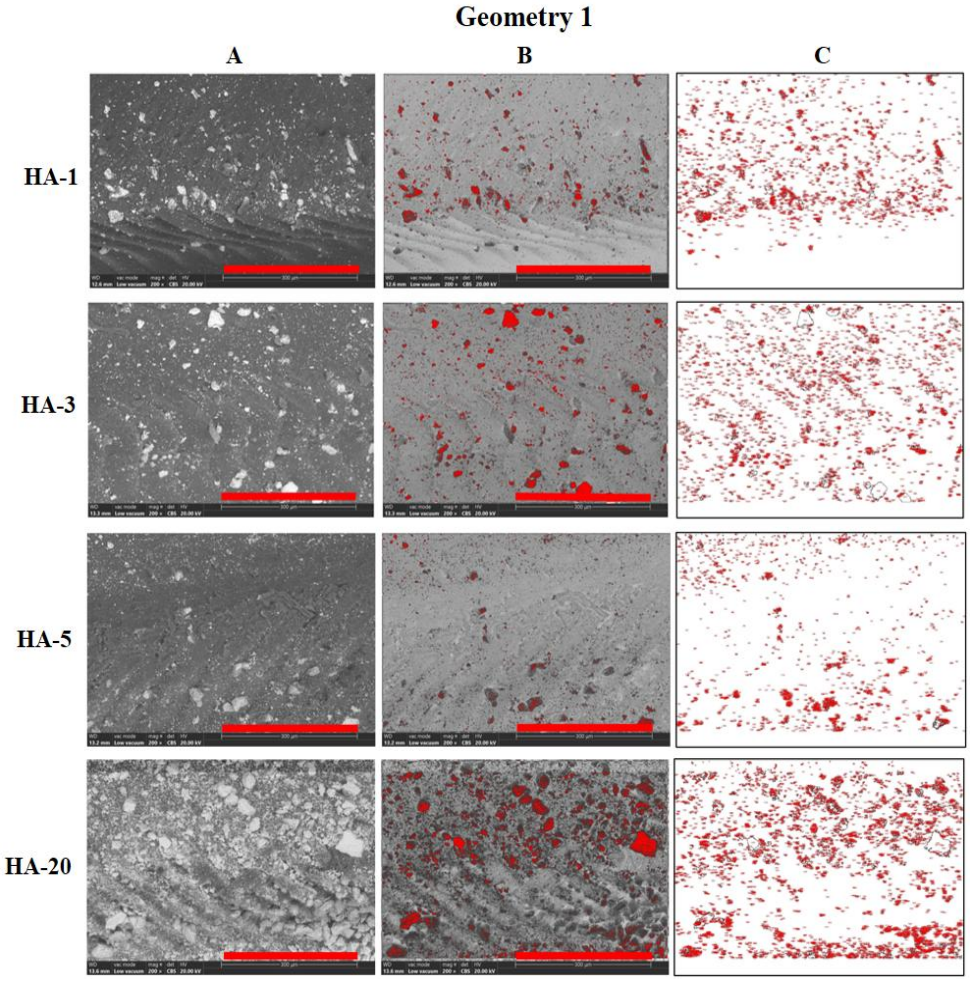

Fig. 7. Representative results obtained after ImageJ processing of SEM images for Geometry 1: A – primary images, B – images after threshold isolation of HA particles, C – HA particle distribution map.Scale bar: 300 μm.

The automated image analysis reveals a direct relationship between the coverage degree and the HA mass concentration (Table 2). At the maximum filler level of 20 wt.% HA, the measured area fraction reached 4.816% in Geometry 1 and 3.510% in Geometry 2 (see Fig. 9).

Table 2

Quantitative parameters of HA particles dispersion on the 3D-printed composite surfaces

Sample Set	Sample	Total Area [μm²]	Average Size [μm²]	Area coverage degree [%]
Geometry 1	HA-1	9886.9	9.096	1.157
	HA-3	10041	8.878	1.175
	HA-5	5352.4	5.564	0.626
	HA-20	24046	13.916	2.813
Geometry 2	HA-1	2807.1	5.094	0.328
	HA-3	43340	33.160	5.071
	HA-5	50069	36.654	5.858
	HA-20	10459	7.917	1.224

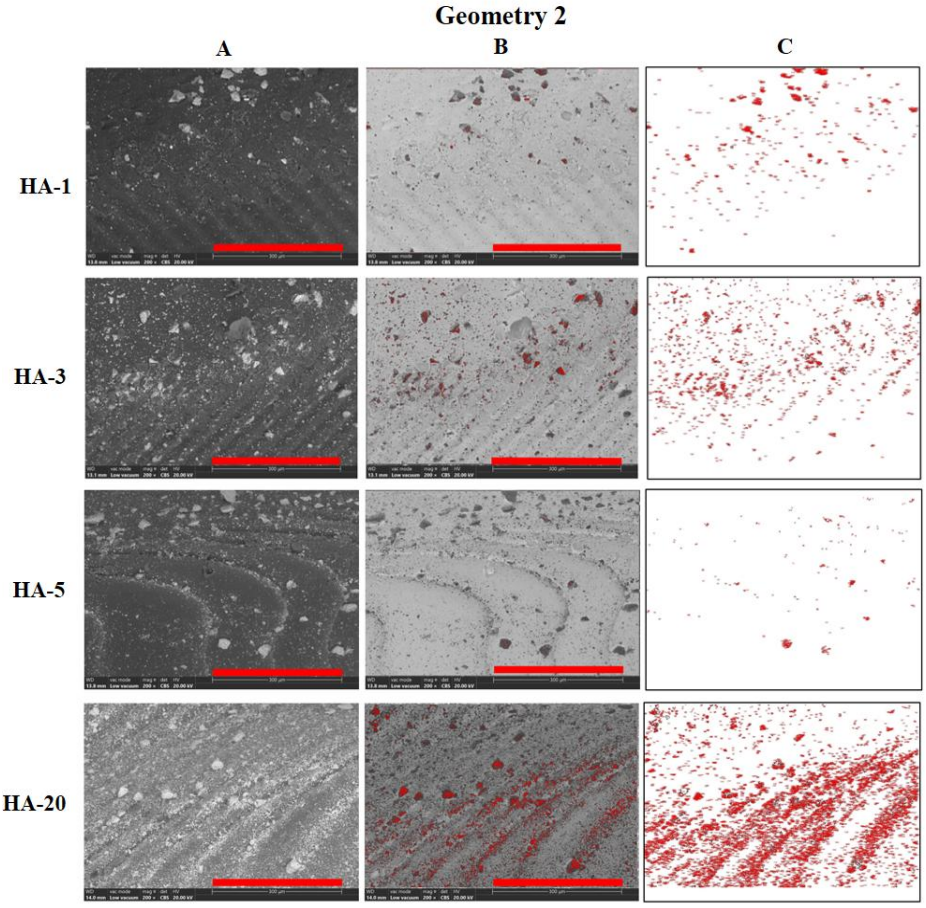

Fig. 8. Representative results obtained after ImageJ processing of SEM images for Geometry 2: A – primary images, B – images after threshold isolation of HA particles, C – HA particle distribution map.Scale bar: 300 μm.

The abovementioned quantitative results substantiate the initial morphological findings, proving that the architectural design of Geometry 1 favours a significantly better dispersion and structural stability of the HA reinforcement compared to Geometry 2. Furthermore, despite the occurrence of localized macroscopic agglomerations at the 20 wt.% HA threshold, the overall dispersion pattern within the entire sample volume proved to be extensive. This ultimately demonstrates that the utilized DLP printing technology successfully incorporated and retained high percentages of bioactive ceramic mass within the photopolymerized matrix.

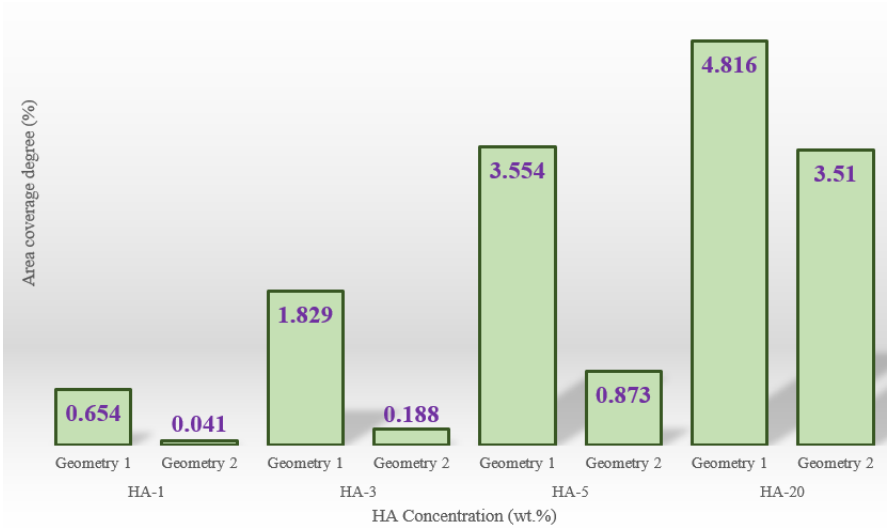

Fig. 9. The degree of dispersion of HA particles in the polymer matrix

6. Conclusions

Utilizing DLP 3D printing to manufacture customized biocomposite osteosynthesis screws introduces a reliable pathway for blending natural bovine HA with a commercial photopolymerizable PLA-based resin. Assessing this integration across varying HA concentrations and two distinct medical geometries revealed microstructural data. Key findings show that while up to 20 wt.% HA can be successfully incorporated without compromising layer print accuracy, a 3 wt.% ratio guarantees the optimal, agglomeration-free particle dispersion. This highly precise manufacturing route directly addresses traditional ceramic-polymer integration challenges, delivering an advanced solution for customized medical implants alongside wide adaptability for other industrial sectors.

REFERENCES

[1] *M. Pagac, et al.*, A review of vat photopolymerization technology: materials, applications, challenges, and future trends of 3D printing, Polymers, Vol. **13**, Iss. 4, 2021, p. 598

[2] *A. Bagheri, J. Jin*, Photopolymerization in 3D printing, ACS Applied Polymer Materials, Vol. **1**, Iss. 4, 2019, pp. 593-611.

[3] *H. Quan, et al.*, Photo-curing 3D printing technique and its challenges, Bioactive materials, Vol. **5**, Iss. 1, 2020, pp. 110-115.

[4] *R. Pugliese, et al.*, Polymeric biomaterials for 3D printing in medicine: An overview, Annals of 3D Printed Medicine, Vol. **2**, 2021, p. 100011.

[5] *A.S. Neto, A. Gaddam, G.E. Stan, J.M.F. Ferreira*, Multifunctional cuttlefish bone–derived scaffolds: Smart biomimetic solutions for bone tissue repair and regeneration, Journal of the American Ceramic Society, Vol. **108**, 2025.

[6] *L.M. Bălescu, Z. Mighri, G.E. Stan*, Porous bioceramic coatings and coatings for porous implants, in Porous Bioceramics for Biomedical Applications (F. Baino, M. Montazerian, Eds.), Elsevier, 2026, pp. 375-416.

[7] *S. Mondal, S. Park, J. Choi, T.T.H. Vu, V.H.M. Doan, T.T. Vo, B. Lee, J. Oh*, Hydroxyapatite: A journey from biomaterials to advanced functional materials, Advances in Colloid and Interface Science, Vol. **321**, 2023, Art. no. 103013.

[8] *F. Miculescu, et al.*, Structural and morphological induced modifications in hydroxyapatite obtained by bone thermal treatments, Journal of Optoelectronics and Advanced Materials, Vol. **17**, Iss. 9-10, 2015, pp. 1361-1366.

[6] *I. Antoniac, V. Mănescu (Păltânea), G. Păltânea, A. Antoniac, I.V. Nemoianu, M.I. Petrescu, H. Dura, A.D. Bodog*, Additive Manufactured Magnesium-Based Scaffolds for Tissue Engineering, Materials, Vol. **15**, Iss. 23, 2022, Art. no. 8693

[7] *A.-C. Mocanu, et al.*, Selection Route of Precursor Materials in 3D Printing Composite Filament Development for Biomedical Applications, Materials, Vol. **16**, Iss. 6, 2023, p. 2359.

[8] *L.A. Drăghici, R.M. Comăneanu, D. Vrânceanu, F. Baciu, M. Stoian-Albulescu, A.M. Dobrescu, T.P. Ionescu, C. Gioga*, Experimental study on the compressive strength of fixed prosthetic restorations on tooth preparations with or without horizontal preparation, Journal of Medicine and Life, Vol. **18**, Iss. 7, 2025, pp. 671-677.

[9] *F. Miculescu, et al.*, Comparative studies regarding heavy elements concentration in human cortical bone, Digest Journal of Nanomaterials and Biostructures, Vol. **6**, Iss. 3, 2011, pp. 1117-1127.

[10] *A. Maidaniuc, et al.*, Sinterability study of bovine-derived hydroxyapatite and silver microcomposites, U.P.B. Sci. Bull., Series B, Vol. **79**, Iss. 1, 2017, pp. 145-154.

[11] *C.-A. Dascălu, et al.*, Synthesis and characterization of biocompatible polymer-ceramic film structures as favorable interface in guided bone regeneration, Applied Surface Science, Vol. **494**, 2019, pp. 335-352.

[12] *A. Maidaniuc, et al.*, Effect of micron sized silver particles concentration on the adhesion induced by sintering and antibacterial properties of hydroxyapatite microcomposites, Journal of Adhesion Science and Technology, Vol. **30**, Iss. 17, 2016, pp. 1829-1841.

[13] *H.W. Kim, H.H. Lee, J. Knowles*, Electrospinning biomedical nanocomposite fibers of hydroxyapatite/poly (lactic acid) for bone regeneration, Journal of Biomedical Materials Research Part A, Vol. **79**, Iss. 3, 2006, pp. 643-649.

[14] *F. Miculescu, et al.*, Experimental researches on biomaterial-tissue interface interactions, Journal of Optoelectronics and Advanced Materials, Vol. **9**, Iss. 11, 2007, pp. 3303-3306.

[15] *J.G. Montagut, A. González, R. Paz, L. Suárez, P. Bordón, Z. Ortega, I. Antoniac, I. Cacciotti, A. Ileana, M. Monzón*, Additive Manufacturing in Dentistry: A Comparative Study of Polymeric Surgical Guide Fabrication, Polymers, Vol. **17**, Iss. 20, 2025, Art. no. 2764.
[16] *F. Miculescu, et al.*, Influence of the modulated two-step synthesis of biogenic hydroxyapatite on biomimetic products' surface, Applied Surface Science, Vol. **438**, 2018, pp. 147-157.
[17] *A.-C. Mocanu, et al.*, Naturally-derived biphasic calcium phosphates through increased phosphorus-based reagent amounts for biomedical applications, Materials, Vol. **12**, Iss. 3, 2019, p. 381.
[18] *F. Miculescu, et al.*, Synthesis and characterization of jellified composites from bovine bone-derived hydroxyapatite and starch as precursors for robocasting, ACS Omega, Vol. **3**, 2018, pp. 1338-1349.
[19] *M. Kozadaeva, D. Khrapov, I.Y. Grubova, A. Vlădescu, V. Anorin, C.M. Cotruț, K. Loukelis, M. Dinu, M. Chatzinikolaidou, F. Kraus, F. Noll, P. Kahler, A.V. Koptyug, R.A. Surmenev, M.A. Surmeneva*, Multiscale design of an additively manufactured Ti–Nb alloy with nanostructured Sr-substituted hydroxyapatite coating for bone tissue engineering, Ceramics International, Vol. **51**, Iss. 25, 2025, pp. 46323-46342
[20] *V. Mitran, et al.*, Osteoblast cell response to naturally derived calcium phosphate-based materials, Materials, Vol. **11**, Iss. 7, 2018, p. 1097.
[21] *A.-C. Mocanu, et al.*, Internal and external surface features of newly developed porous ceramics with random interconnected 3D channels by a fibrous sacrificial porogen method, Applied Surface Science, Vol. **489**, 2019, pp. 226-238.
[22] *B.J. Inkson*, Scanning electron microscopy (SEM) and transmission electron microscopy (TEM) for materials characterization, in Materials characterization using nondestructive evaluation (NDE) methods, Elsevier, 2016, pp. 17-43.
[23] *J. Hamuyuni, M.O. Daramola, O.O. Oluwasina*, Energy-Dispersive X-Ray Spectroscopy: Theory and Application in Engineering and Science, Encyclopedia of Physical Organic Chemistry, 2016, pp. 1-23.
[24] *A.-C. Mocanu, F. Miculescu, M.-A. Pandele, E.-S. Dondea, Ș.I. Voicu, A.A. Dobre, A. Ghebaur, L.-T. Ciocan*, Induced antibacterial activity of printable composite materials: Influence of the conjoined modulation of ampicillin/hydroxyapatite/graphene nanoplatelets ratios, Ceramics International, Vol. **51**, Iss. 4, 2025, pp. 5181-5198.